High-efficiency organic electroluminescent materials based on D-A-D type with sterically hindered methyl groups

Youming Zhang,[ab] Xuan Zhou,[ad] Changjiang Zhou,[b] Qiang Su,[c] Shuming Chen,[c]* Jun Song[d] and Wai-Yeung Wong[a]*

[a] *Department of Applied Biology and Chemical Technology, The Hong Kong Polytechnic University, Hung Hom, Hong Kong, P. R. China*

[b] *College of Materials Science and Engineering, Shenzhen University, Shenzhen 518060, China*

[c] *Department of Electrical and Electronic Engineering, Southern University of Science and Technology, Shenzhen, 518055, P. R. China*

[d] *Key Laboratory of Optoelectronic Devices and Systems of Ministry of Education and Guangdong Province, College of Physics and Optoelectronic Engineering, Shenzhen University, Shenzhen 518060, P. R. China*

E-mail: wai-yeung.wong@polyu.edu.hk; chen.sm@sustc.edu.cn

Abstract: Three donor-acceptor-donor type emitters of **2TPA-BT**, **2MeTPA-BT** and **2DMeTPA-BT** were synthesized. Crystal structures for all compounds were determined by single-crystal X-ray diffraction analysis, showing that by introducing one or two methyl groups between the donors and acceptor, the spatial configuration changes greatly for **2MeTPA-BT** and **2DMeTPA-BT** compared to their parent compound **2TPA-BT**. Density functional theory analysis reveals that the emission of **2MeTPA-BT** has a more obvious hybridized local and charge-transfer (HLCT) feature based on the influence of steric hindrance of methyl substituents. Attributed to their different spatial configurations and luminescence mechanisms, different emission wavelengths with high photoluminescent quantum yields (Φ_{PL}s) of 75.43%, 93.43% and 89.63% in toluene solvent, as well as 44.76%, 52.19 and 33.87% in neat film were observed for **2TPA-BT**, **2MeTPA-BT** and **2DMeTPA-BT**, respectively. Furthermore, strong electroluminescence was observed with the emission peaks at 602, 560 and 544 nm, maximum current efficiencies of 11.05 cd/A, 30.40 cd/A and 25.02 cd/A, maximum power efficiencies of 6.01 lm/W, 23.67 lm/W and 20.37 lm/W, maximum external quantum efficiencies 4.43%, 8.47% and 7.29% for **2TPA-BT**, **2MeTPA-BT** and **2DMeTPA-BT** doped organic light-emitting devices (OLEDs), respectively. This work clearly illustrates the effect of spatial configuration changes on the luminescence properties of organic emitters.

Keywords: spatial configuration, hybridized local and charge-transfer, organic light-emitting diodes, electroluminescence, crystal structure.

Introduction

Organic light-emitting diodes (OLEDs) have been heavily studied in the past few decades. To date, great progress has been made in the research of organic electroluminescent materials and the electroluminescence efficiency records of materials are constantly being refreshed.[1-5] According to spin quantum theory, the ratio of the singlet and triplet exciton is 1:3 for the composite processes. Therefore, harvesting 75% of the triplet exciton energy is the key factor to obtain highly efficient devices.[5-8] Phosphorescent complexes have attracted much attention because they can provide a transition channel from a triplet state to a ground state and can directly capture 100% internal quantum efficiency. Devices using phosphorescent complexes can usually achieve high luminescence efficiency. [9-11] For example, recently, Zheng *et al*. reported three cyclometalated iridium(III) complexes which achieved an extremely high photoluminescent quantum yield (Φ_{PL}) over 90% in dichloromethane and maximum external quantum efficiency (EQE_{max}) over 30% in their related OLEDs.[2] However, metal complexes are commonly associated with air- and moisture-instability, environmental toxicity and high cost. In view of this, the design and synthesis of highly efficient, low cost and low pollution metal-free emitters is still a huge challenge.

Compared to phosphorescent materials, metal-free organic materials have garnered great research interest due to their advantages of fluorescent nature (to avoid the quenching of long-lifetime excitons), molecular diversity, low cost, and tunable energy gap, as well as the capability for mass production.[7, 12] New hybridized local

and charge-transfer state (HLCT) and thermally activated delayed fluorescence (TADF) materials have been proposed to harvest both singlet and triplet excitons and break the 5% EQE limit in OLED devices by controlling the excited state with both local excitation (LE) and charge transfer (CT) features and regulating orbital separation between the highest occupied molecular orbital (HOMO) and the lowest unoccupied molecular orbital (LUMO).[13-18] For TADF, the value of S_1–T_1 energy gap (ΔE_{ST}) is the most important factor for the photophysical and electroluminescence properties. The smaller ΔE_{ST} is beneficial for harvesting the triplet excitons via reverse intersystem crossing (RISC). For HLCT emission, the intersystem crossing of excitons between triplet state T_m and singlet state S_n with close energy levels can also occur in the excited state. This state combines both local excited (LE) and charge transfer (CT) states into a special one, possessing two combined and compatible characteristics: a large transition moment from the LE state (cold exciton) and a weakly bound exciton from the CT state ("hot" exciton).

Based on these luminescence mechanisms, scientists have developed many highly efficient metal-free electrofluorescent emitters. Generally, a large separation between HOMO and LUMO can decrease the energy gap of T_m and S_n, and increase the RISC rate, which is the key factor for HLCT emission.[19-22] Therefore, HLCT is often observed in intramolecular charge transfer (ICT) systems containing spatially separated donor (D) and acceptor (A) moieties.[23-30] Theoretically, the spatial geometry, especially the spatial arrangement between the D and A units, has a great influence on the distributions of HOMO and LUMO. Thus, regulating the spatial

distribution of D and A units is an effective strategy to obtain highly efficient electrofluorescent materials.

Considering the above considerations, to further validate our hypothesis, we use the traditional D-A-D type molecule, **2TPA-BT**, as a reference. By wisely introducing sterically hindered methyl groups between the D and A units, two new chromophores of **2MeTPA-BT** and **2DMeTPA-BT** are designed and synthesized, where triphenylamine (TPA) and benzothiadiazole (BT) are used as the D and A units, respectively. Figure 1 shows their chemical structures. Due to the steric hindrance, the torsional angles of the D and A units of the three molecules are quite different. Torsional angles between D and A units of ~ 32°, ~ 58° and ~ 84° are observed for **2TPA-BT**, **2MeTPA-BT** and **2DMeTPA-BT** by single-crystal X-ray diffraction analysis. Further density functional theory (DFT) analysis reveals that the emission of **2MeTPA-BT** has more obvious hybridized local and charge-transfer (HLCT) feature based on the influence of steric hindrance of methyl groups. Attributed to their different spatial configurations and luminescence mechanisms, different emission wavelengths with high photoluminescent quantum yields (Φ_{PL}s) were observed in both organic solvents and neat film of **2MeTPA-BT** and **2DMeTPA-BT**. Moreover, the corresponding OLEDs displayed strong electroluminescence (EL) with high efficiencies. Our work clearly illustrates the effect of spatial configuration changes on the luminescence properties of the organic emitters.

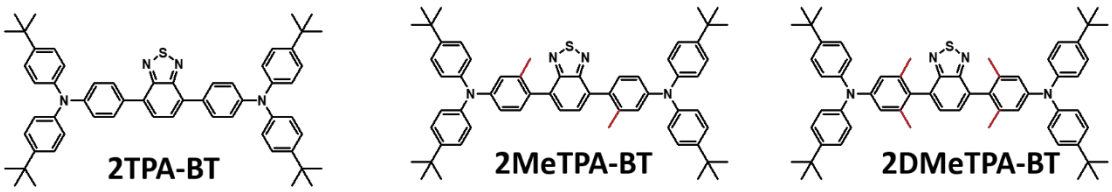

Figure 1. Chemical structures of **2TPA-BT**, **2MeTPA-BT** and **2DMeTPA-BT**.

Results and discussion

Synthesis and thermal stability

The starting materials 1-*tert*-butyl-4-iodobenzene, 4-bromo-3-methylbenzenamine, 4-bromo-3,5-dimethylbenzenamine,4,7-bis(4,4,5,5-tetramethyl-1,3,2-dioxaborolan-2-yl)benzo[*c*][1,2,5]thiadiazole (**BT-2Bpin**) and N-(4-bromophenyl)-4-*tert*-butyl-N-(4-*tert*-butylphenyl)benzenamine (**TPA-Br**) (Figure S1), as well as the solvents, were purchased commercially and used as received. All manipulations involving air-sensitive reagents were performed under nitrogen. Compounds of **MeTPA-Br** and **DMeTPA-Br** were synthesized by the Pd-catalyzed C−N cross-coupling reactions.[31] The final products of **2TPA-BT**, **2MeTPA-BT** and **2DMeTPA-BT** were prepared using the common Suzuki coupling reaction using $Pd(PPh_3)_4$ catalyst.[32] All the new intermediates and final products were characterized using NMR (^1H and ^{13}C) spectroscopy and mass spectrometry, confirming their well-defined chemical structures. Detailed synthesis methods are provided in the supporting information.

Figure 2 shows the results of thermogravimetric analysis for these emitters under a N_2 atmosphere, and the related data are given in Table 1. The decomposition temperature (T_d) was found to be 471 °C, 460 °C and 448 °C for **2TPA-BT**, **2MeTPA-BT** and **2DMeTPA-BT**, respectively, at 5% weight loss, which reveals that

these organic emitters have sufficiently high thermal stability useful for the fabrication of OLEDs.

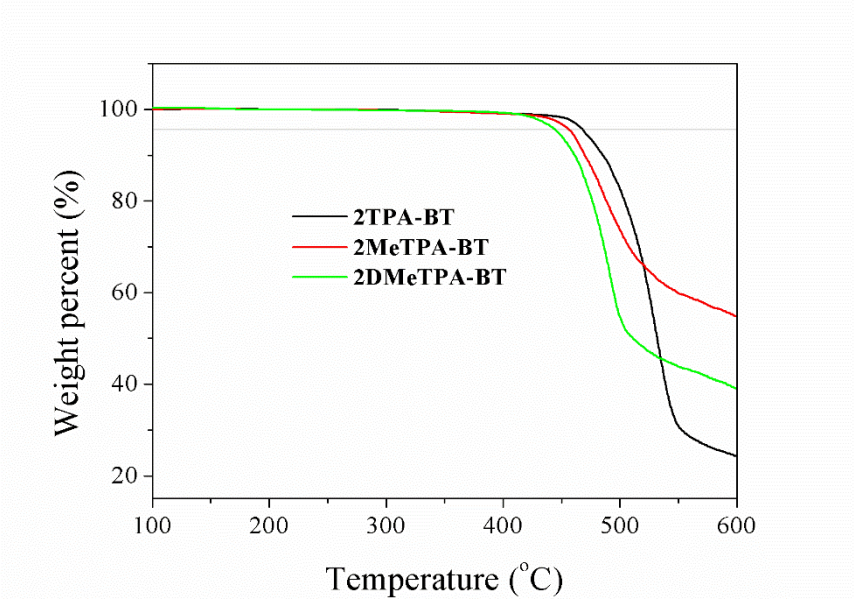

Figure 2. Thermogravimetric analysis curves for **2TPA-BT**, **2MeTPA-BT** and **2DMeTPA-BT**.

Crystal structures

Crystals of all final products were obtained by slow diffusion of methanol into their dichloromethane (DCM) solutions. Figure 3 shows the front view and side view of the thermal ellipsoid drawings from X-ray analysis. All of the emitters displayed a highly twisted molecular conformation with torsional angles between D and A units of ~ 32°, ~ 58° and ~ 84° for **2TPA-BT**, **2MeTPA-BT** and **2DMeTPA-BT** due to the presence of the methyl groups, which affect the degree of conjugation, resulting in different emission wavelengths. There are intramolecular and/or intermolecular C-H···N hydrogen bonds for these emitters. For **2TPA-BT**, hydrogen bonds were formed between the nitrogen atom on the BT group and hydrogen atoms on the TPA group of intramolecular and adjacent molecule with distances of 2.566 and 2.885 Å (Figure

3a). For **2MeTPA-BT**, intramolecular C-H···N hydrogen bonds were formed between one of the nitrogen atoms on the BT group and hydrogen atom on the benzene ring, as well as the hydrogen atom on the methyl group of the TPA group with distances of 2.577 and 2.481 Å. Furthermore, due to the influence of steric hindrance of the methyl substituent, the hydrogen atoms on the phenyl ring and methyl group of the TPA group has a closer distance of 2.441 and 2.543 Å than that of **2TPA-BT** to the nitrogen atom of the neighboring molecule, which can form stronger intermolecular C-H···N hydrogen bonds (Figure 3b), which also has a favorable influence on the luminescent properties. For **2DMeTPA-BT**, the huge torsional angles between the D and A units lead to large distances of 3.871 and 6.770 Å between the nitrogen atom on the BT group and the hydrogen atom on the methyl group of intramolecular and intermolecular TPA, which only formed weak intramolecular C-H···N hydrogen bonds (Figure 3c). The crystal data and structure refinements for all emitters are summarized in Table S1.

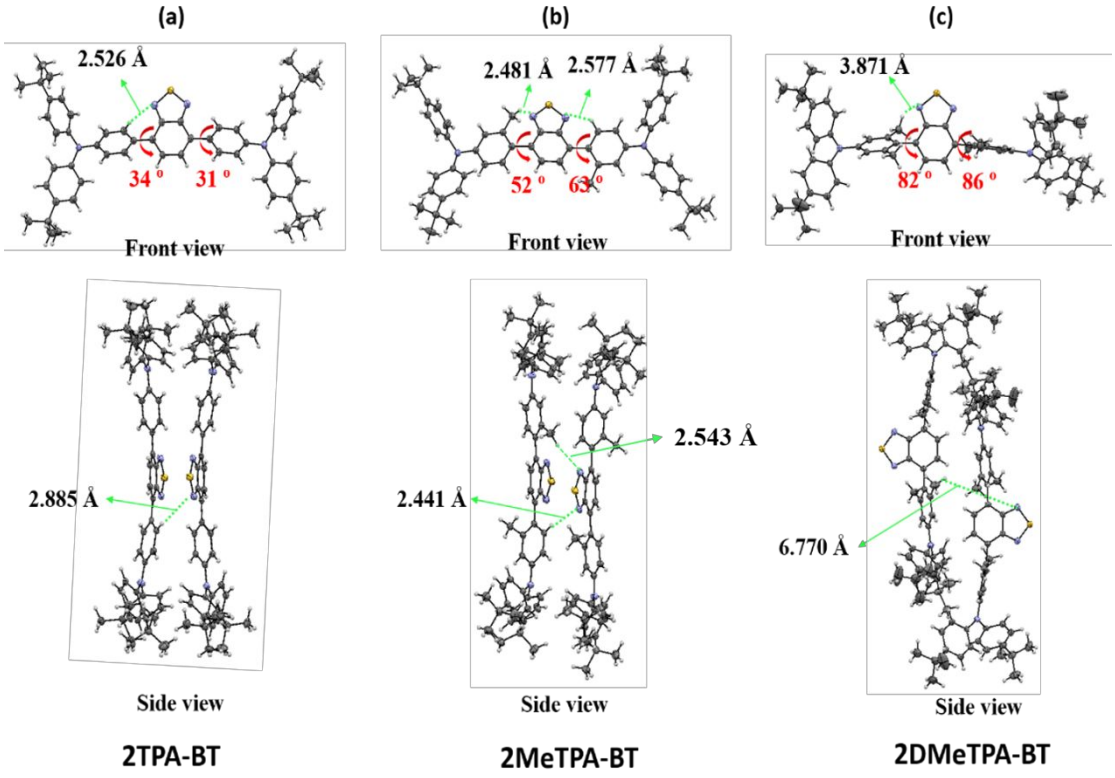

Figure 3. Thermal ellipsoid plots with 30% probability. The hydrogen atoms are omitted for clarity. (CCDC no. 1890911, 1890912 and 1890913 for **2TPA-BT**, **2MeTPA-BT** and **2DMeTPA-BT**, respectively.)

Electrochemical properties

Cyclic voltammetry (CV) curves for **2TPA-BT**, **2MeTPA-BT** and **2DMeTPA-BT** were measured as neat films coated on a platinum electrode as shown in Figure 4. Related data are collected in Table 1. The empirical relationship $E_{HOMO} = [-E_{ox} - 4.8]$ eV and $E_{LUMO} = [-E_{red} - 4.8]$ eV were applied to estimate the HOMO energy level (E_{HOMO}) and LUMO energy level (E_{LUMO}) by the onset oxidation/reduction potentials (E_{ox}/E_{red}), where 4.8 eV is the energy level of ferrocene with respect to the vacuum energy level.[33] Three reversible redox couples of 0.37/-1.80, 0.41/-1.93 and 0.47/-1.95 V vs ferrocene were found for **2TPA-BT**, **2MeTPA-BT** and

2DMeTPA-BT, respectively, which can be attributed to the first oxidation of the TPA units and the first reduction of the BT unit.[34] It is worth noting that with increasing torsional resistance of the molecular species due to spatial effects, the oxidation potentials of the emitters also increased, and the reduction potentials decreased successively. Here, the introduction of methyl group can not only enhance the ability of electron donating, but also change the configuration of the molecule to a large extent. This may be the reason why the oxidation potential is increased in the order of **2DMeTPA-BT** > **2MeTPA-BT** > **2TPA-BT**. Ultimately, this leads to the gradually increasing electrochemical band gaps (*E*g cv) of 2.17, 2.34 and 2.42 eV for **2TPA-BT**, **2MeTPA-BT** and **2DMeTPA-BT**, respectively.

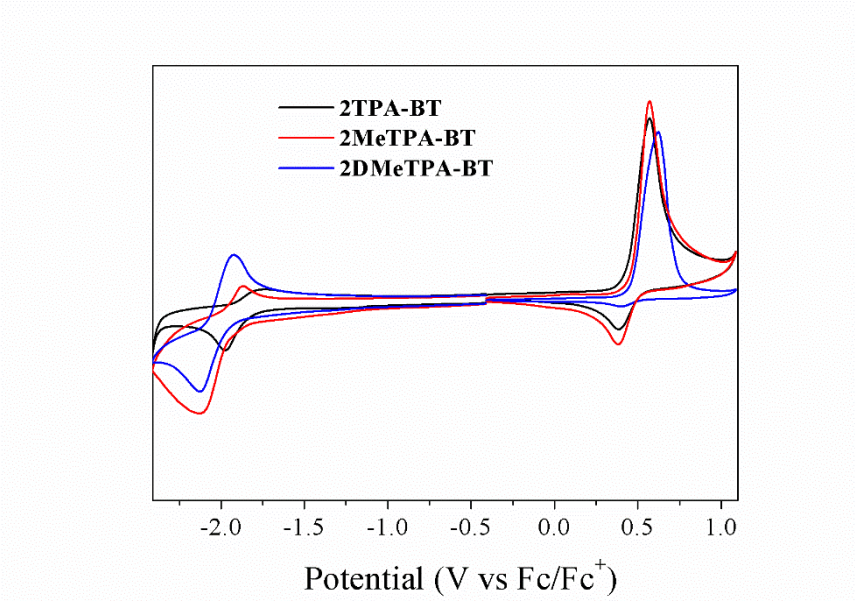

Figure 4. Cyclic voltammograms for emitter films on a platinum electrode in an acetonitrile solution containing 0.1 mol L^{-1} Bu_4NPF_6 at 100 mV s^{-1} scan rate using ferrocene internal standard.

Table 1. Thermal stability and electrochemical data for the three emitters.

Emitters	E_{ox}[a]/V	E_{red}[a]/V	E_{HOMO}[b]/eV	E_{LUMO}[b]/eV	E_{cv}/eV	T_d /°C
2TPA-BT	0.37	-1.80	-5.17	-3.00	2.17	471
2MeTPA-BT	0.41	-1.93	-5.21	-2.87	2.34	460
2DMeTPA-BT	0.47	-1.95	-5.27	-2.85	2.42	448

[a] Onset oxidation and reduction potentials measured by cyclic voltammetry in solid films. [b] E_{HOMO} = [$-E_{ox}$ – 4.8] eV, E_{LUMO} = [$-E_{red}$ – 4.8] eV, where 4.8 eV is the energy level of ferrocene relative to the vacuum energy level.

Photophysical properties

The UV–vis absorption and fluorescence spectra of **2TPA-BT**, **2MeTPA-BT** and **2DMeTPA-BT** in different polar solvents are shown in Figure 5 and the relevant data are summarized in Table 2. Intense high energy absorption bands were assigned to the intramolecular π-π* electronic transition. Low energy absorption bands were attributed to intramolecular charge transfer (ICT) transitions from D to A units. Strong intramolecular π-π* electronic absorptions occurred at approximately 310 nm for all the three emitters, but different ICT absorption bands were observed (approximately 470, 435 and 425 nm for **2TPA-BT**, **2MeTPA-BT** and **2DMeTPA-BT**, respectively). The intensity of ICT absorption bands gradually decreased in the order of 2**TPA-BT** > **2MeTPA-BT** > **2DMeTPA-BT** due to the increase of torsion in molecular space. This clearly indicates that intramolecular interactions between D and A units correspondingly decreased and were induced by the introduced methyl groups. Moreover, these emitters shared similar absorption profiles and the absorption maxima changed only very little with the solvent polarities, implying a rather small dipolar change in the ground state for different solvents.[35] Red-shifted absorption spectra were obtained in the solution and neat films due to their intermolecular interaction (Figure S2). Based on the film absorption onsets, we calculated the optical band gaps (*E*opt g) as 1.93, 2.07 and 2.45 eV for

2TPA-BT, **2MeTPA-BT** and **2DMeTPA-BT**, respectively. The calculated values are in good agreement with the electrochemical band gap sequence.

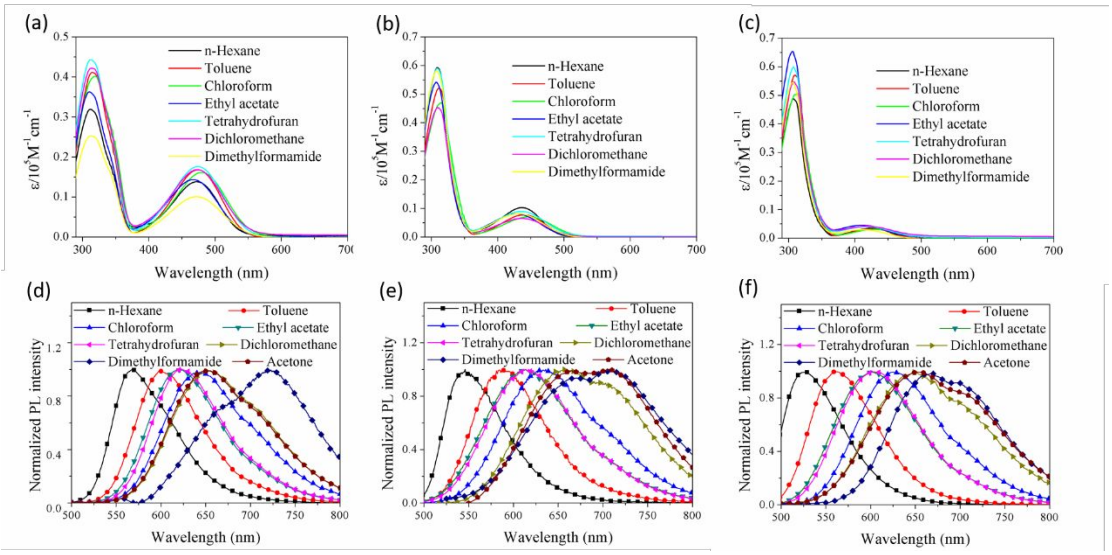

Figure 5. UV-vis absorption and photoluminescence spectra in different solvents. (a)/(d) for **2TPA-BT**, (b)/(e) for **2MeTPA-BT** and (c)/(f) for **2DMeTPA-BT**, respectively.

Figure 5d–5f show the photoluminescence (PL) spectra of the emitters in different solvents. In contrast to the absorption properties, fluorescence spectra were broadened and exhibited remarkable redshifts as the solvent polarity increased. Emission peaks shifted from 569, 546 and 528 nm in non-polar hexane to 723, 710 and 670 nm in polar dimethylformamide for **2TPA-BT**, **2MeTPA-BT** and **2DMeTPA-BT**, respectively. This large solvatochromic shift indicates a strong ICT state.[36] Also, the neat film of emitters produced an emission peak at 611, 567 and 548 nm for **2TPA-BT**, **2MeTPA-BT** and **2DMeTPA-BT**, respectively (Figure S3). Correspondingly, the Φ_{PL}s of the emitters in toluene with 75.43%, 93.43% and 89.63%, as well as neat films with 44.76%, 52.19% and 33.87% were recorded for **2TPA-BT**, **2MeTPA-BT** and **2DMeTPA-BT**, respectively. The reduced Φ_{PL}s in neat films indicate that these emitters suffer from aggregation-caused quenching (ACQ)

due to intermolecular stacking, which is a common phenomenon of organic luminogens. As a consequence, the radiative transition rate (k_r) was calculated to be 1.27×10^8, 1.67×10^8 and 1.23×10^8 s^{-1} in toluene solution, as well as 0.83×10^8, 1.11×10^8 and 0.33×10^8 s^{-1} in neat film for **2TPA-BT**, 2**MeTPA-BT** and **2DMeTPA-BT**. The nonradiative decay (k_{nr}) was calculated to be 0.41×10^8, 0.12×10^8 and 0.14×10^8 s^{-1} in toluene solution, as well as 1.02×10^8, 1.11×10^8 and 0.61×10^8 s^{-1} in neat film for **2TPA-BT**, **2MeTPA-BT** and **2DMeTPA-BT**, respectively. The k_r of 2**MeTPA-BT** is larger than the other two values as a result of the molecular configurational regulation.

We used the Lippert-Mataga expression to better understand the relationship between the Stokes shift and solvent polarity parameter (Δf) to evaluate the ICT effect.[8, 27, 37-38] As shown in Figure 6, emitters of **2TPA-BT** and **2MeTPA-BT** exhibited two-section linear relations in low- and high-polarity solvents. The dipole moment (μ_e) of 15.2 and 18.6 D in low polarity solvents, as well as 31.7 and 30.2 D in high polarity solvents, were calculated for **2TPA-BT** and **2MeTPA-BT**, respectively. Similar to the related references, the smaller μ_e in less polar solvents is attributed to the locally excited (LE) state, while the larger μ_e in highly polar solvents is assigned to the charge-transfer (CT) excited state.[39-40] The HLCT state is formed through the coupling and intercrossing between the CT and LE states. However, compared to **2TPA-BT** and **2MeTPA-BT**, which have two one-section linear relation in low- and high-polarity solvents, there is only a one-section linear relation for **2DMeTPA-BT**, suggesting no HLCT emission for **2DMeTPA-BT**. Moreover, time-resolved

experiments revealed a monoexponential decay of S_1 state in low polarity solvents (toluene, Figure 6d) implying that LE and CT components of emitters were combined into the HLCT state. Also, there is no long lifetime state that can be detected in neat films, suggesting these emitters are not delayed fluorescence emitters (Figure S4).

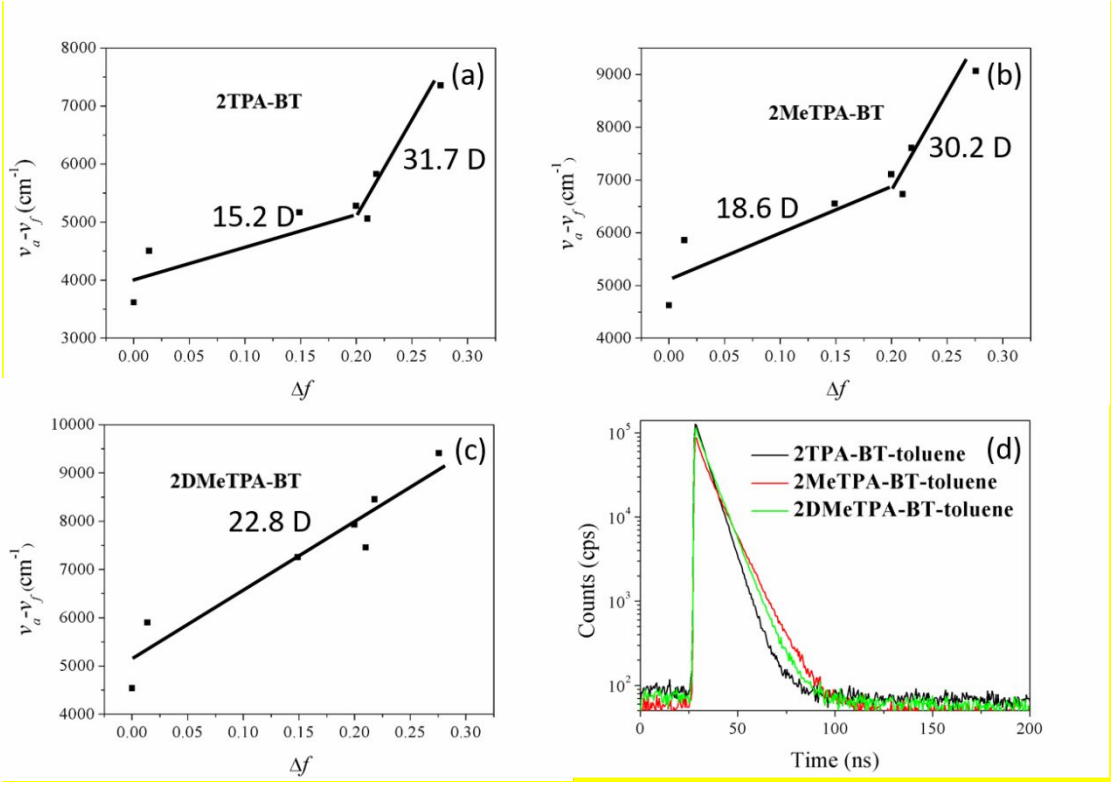

Figure 6. Linear correlation of orientation polarity Δf of solvent media with Stokes shift (ν_a–ν_f) for (a) **2TPA-BT**, (b) **2MeTPA-BT** and (c) **2DMeTPA-BT**. Transient photoluminescence decay spectra of emitters in toluene (d).

Table 2. Photophysical properties for the three emitters

Emitters	Solvents	λabs sol/nm [a]	λabs film /nm [b]	λem sol/nm [a]	λem film / nm [b]	*E*opt g/ eV [c]	Φ_{pl}/ (%) sol/film [d]	τ/ns sol/film	$k_r/10^8$ (s^{-1}) sol/film	$k_{nr}/10^8$ (s^{-1}) sol/film
2TPA-BT	n-Hexane	472, 311	498, 329	569	611	1.93	75.43 (toluene) /44.76 (neat film)	5.91 (toluene) /5.40 (neat film)	1.27 (toluene) /0.83 (neat film)	0.41 (toluene) /1.02 (neat film)
	Toluene	473, 312		601						
	Ethyl acetate	466, 310		618						
	Tetrahydrofuran	472, 313		620						
	Dichloromethane	481, 318		651						
	Chloroform	481, 318		640						
	Dimethylformamide	472, 315		723						
2MeTPA-BT	n-Hexane	436, 307	446, 320	546	567	2.07	93.43 (toluene) /52.19 (neat film)	5.29 (toluene) /4.63 (neat film)	1.76 (toluene) /1.11 (neat film)	0.12 (toluene) /1.01 (neat film)
	Toluene	439, 311		591						
	Ethyl acetate	428, 309		615						
	Tetrahydrofuran	435, 309		615						
	Dichloromethane	435, 309		690						
	Chloroform	446, 314		636						
	Dimethylformamide	432, 307		710						
2DMeTPA-BT	n-Hexane	426, 306	430, 320	528	548	2.45	89.63 (toluene) /33.87 (neat film)	7.28 (toluene) /10.26 (neat film)	1.23 (toluene) /0.33 (neat film)	0.14 (toluene) /0.61 (neat film)
	Toluene	426, 310		569						
	Ethyl acetate	408, 306		603						
	Tetrahydrofuran	416, 307		603						
	Dichloromethane	420, 308		651						
	Chloroform	432, 313		629						

	Dimethylformamide	411, 307	670

[a] Measured in solution (10^{-5} mol L^{-1}); [b] Measured in neat film; [c] Optical band gaps were determined using *E*opt g, film = $1240/\lambda_{onset,\ film}$; [d] Absolute PL quantum yield measured using an integrating sphere.

Theoretical calculations

We performed DFT calculations using the Gaussian 09 suite of programs at the B3LYP/6-31G(d) level to better understand the electronic and photophysical properties of the emitters at the molecular level.[41] Figure 7a shows that the HOMO of the emitters are mainly located on the D units and the LUMO levels are mostly distributed on the A unit. As we expected, with the increase of torsion in the molecular space, the LUMO are gradually centralized toward the central A unit, while the HOMO are more dispersed on the D units. Thus, the overlap of HOMO and LUMO orbitals are effectively regulated, which should have an effect in the luminescence mechanism of emitters. The molecular band gaps were estimated using DFT as 2.46, 2.52 and 2.59 eV for **2TPA-BT**, **2MeTPA-BT** and **2DMe TPA-BT**, respectively, which are consistent with the experimental data.

To further describe the excited state properties of emitters, we also calculated the natural transition orbital (NTO) of the singlet and triplet states to analyze the electron transition characters (Figures 7b and S5-S7). For the singlet state (S_1 and S_2) of **2TPA-BT**, the holes are dispersed on the whole molecule, and the particles are centralized on the central A component, suggesting the existence of both CT and LE states. But for the singlet state (S_1 and S_2) of **2MeTPA-BT** and **2DMeTPA-BT**, the holes and particles are respectively centralized on the D and A components, implying there is only the CT state. For the triplet state of **2TPA-BT** and **2DMeTPA-BT**, the overlap of distribution for holes and particles demonstrated the coexistence of CT and LE components. But for the T_2 of **2MeTPA-BT**, both of the holes and particles are

centralized on the central A component, which only presents strong the LE state. Thus, the HLCT state for **2MeTPA-BT** can be formed through the coupling and intercrossing between the separate CT and LE states. Clearly, there are large energy gaps of 0.79 and 0.90 eV between T_2 and T_1, as well as energy gaps of 0.89 and 1.10 eV between S_1 and T_1 for **2TPA-BT** and **2MeTPA-BT**, respectively. These large energy gaps may suppress the internal conversion rate of $T_2 \rightarrow T_1$ and the RISC rate of $T_1 \rightarrow S_1$ according to the energy-gap law. However, the larger energy gap between triplet (T_1, T_2 and T_3) and S_1 can also suppress the RISC process for **2DMeTPA-BT,** which would not give the HLCT emission. On the other hand, small energy gaps between S_1 (and/or S_2) and T_2 (or T_3) were obtained for **2TPA-BT** and **2MeTPA-BT**, which could facilitate the RISC process from T_2 (and/or T_3) to S_1 (and/or S_2). These characteristics of NTOs and excited energy levels are well in accordance with the "hot excitons" principle, which would lead to high production efficiency of radiative singlet excitons (η_s) for **2TPA-BT** and **2MeTPA-BT**. The largest energy gap between T_2 and T_1, as well as the smallest energy gaps between S_1 (S_2) and T_2 (T_3) for **2MeTPA-BT** among the three emitters are more beneficial to the RISC process. The computed SOC matrix element values of $\langle S_1\hat{H}SOCT_3\rangle$ for **2TPA-BT**, $\langle S_1\hat{H}SOCT_3\rangle$ for **2MeTPA-BT** and $\langle S_1\hat{H}SOCT_5\rangle$ for **2DMeTPA-BT** are 0.39 cm^{-1}, 0.26 cm^{-1} and 1.84 cm^{-1}, respectively. The results seem to be inconsistent with the experimental data. Although the larger value of SOC may lead to a more enhanced RISC efficiency, the energy gap between singlet and triplet states is still the critical factor for the HLCT emitters. For **2TPA-BT** and **2DMeTPA-BT**, the triplet energy can decay

rapidly from the high-lying triplet state to the low-lying triplet state due to the small energy gap, i.e. energy transfer from T_3 to T_2 for **2TPA-BT,** and T_5 to T_n (n = 2, 3, 4) for **2DMeTPA-BT,** which can also suppress the RISC process.

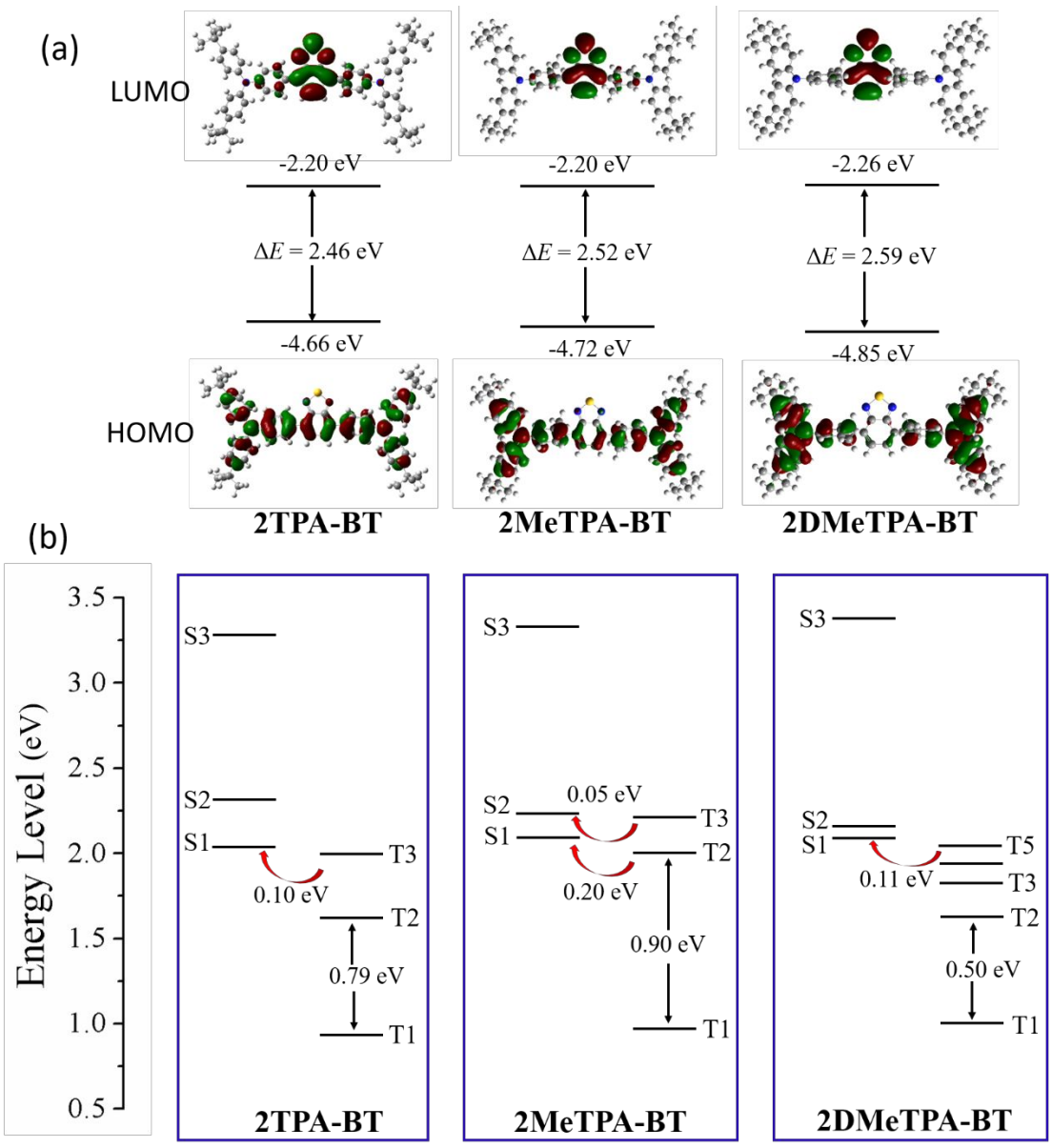

Figure 7. (a) The optimized structure and the calculated HOMO/LUMO spatial distributions of emitters. (b) The energy level of S_1, S_2, T_1, T_2 and T_3.

Electroluminescence properties

To further explore their electroluminescence (EL) properties, OLEDs were fabricated by utilizing the three emitters as dopants with configuration: indium tin

oxide ITO/dipyrazino[2,3-*f*:2′,3′-*h*]quinoxaline-2,3,6,7,10,11-hexacarbonitrile (HATCN, 20 nm)/1,1-bis[4-[*N*,*N*′-di(*p*-tolyl)amino]-phenyl]cyclohexane (TAPC, 40 nm)/emitter: 1,3-di-9-carbazolylbenzene (*m*CP, 5 wt%, 15 nm)/1,3,5-tri[(3-pyridyl)phen-3-yl]benzene (TmPyPB, 50 nm)/LiF (1 nm)/Al (100 nm), where mCP, HATCN, TAPC and TmPyPB served as the host material, hole injection, hole transporting and electron transporting layers, respectively. Figure 8 shows the resulting EL spectra. The devices gave the emission peaks at 602, 560 and 544 nm for **2TPA-BT**, **2MeTPA-BT** and **2DMeTPA-BT** based OLEDs, respectively. Compared to **2TPA-BT**, the EL peaks of **2MeTPA-BT** and **2DMeTPA-BT** based OLEDs show an obvious blue shift of 42 and 58 nm, which are slightly blue shifted from the PL maxima for the corresponding neat films.

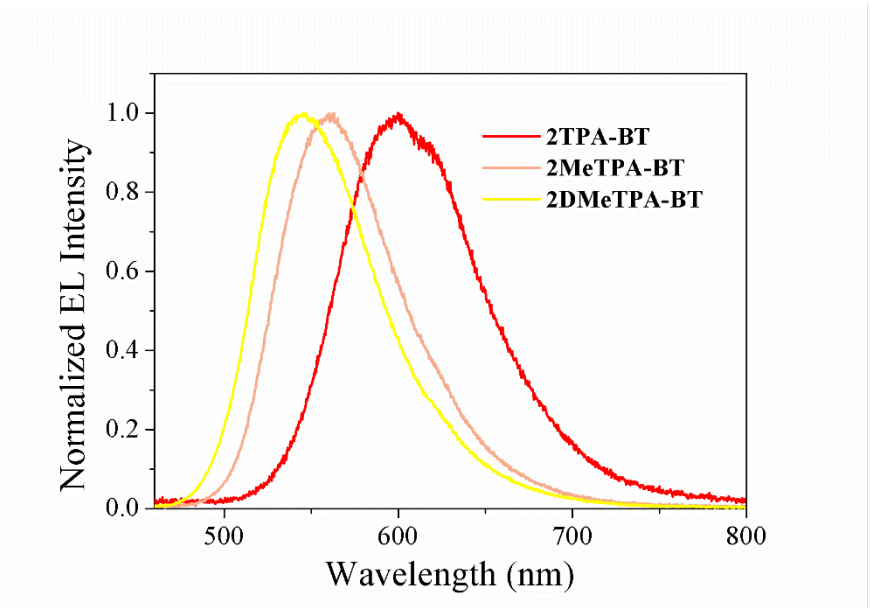

Figure 8. Electroluminescence (EL) spectra for the doped devices of the emitters

Figure 9 shows the current density–voltage–luminance (*J*-*V*-*L*), current efficiency-current density (CE-*J*), power efficiency-current density (PE-*J*) and

quantum efficiency-current density (EQE-*J*) curves, exhibiting Commission Internationale de L'Eclairage (CIE) coordinates of (0.52, 0.47), (0.44, 0.55) and (0.44, 0.55), turn-on voltage (V_{on}) of 4.2, 3.8 and 3.8 V, and maximum luminance (L_{max}) of 26767, 40151 and 64947 cd/m^2 for **2TPA-BT**, **2MeTPA-BT** and **2DMeTPA-BT** doped devices, respectively. The devices exhibited high maximum current efficiencies (CEs) of 11.05 cd/A, 30.40 cd/A and 25.02 cd/A, maximum power efficiencies (PEs) of 6.01 lm/W, 23.67 lm/W and 20.37 lm/W, maximum external quantum efficiencies (EQEs) of 4.43%, 8.47% and 7.29% for **2TPA-BT**, **2MeTPA-BT** and **2DMeTPA-BT** doped OLEDs, respectively. Furthermore, the Φ_{PL}s of the active layer composed of emitter:*m*CP (5 wt%) were measured, values of 39.46%, 69.38% and 44.76% were obtained for the **2TPA-BT**, **2MeTPA-BT** and **2DMeTPA-BT** doped films, respectively (Figures S8-10). It is worth noting that although the EL and PL peaks of **2TPA-BT**, **2MeTPA-BT** and **2DMeTPA-BT** show a gradual blue shift, the emitter of **2MeTPA-BT** has the best luminous efficiency. This result should be also attributed to the regulation of the molecular spatial configuration by introducing sterically hindered methyl groups. The EL data for all the emitters are summarized in Table 3.

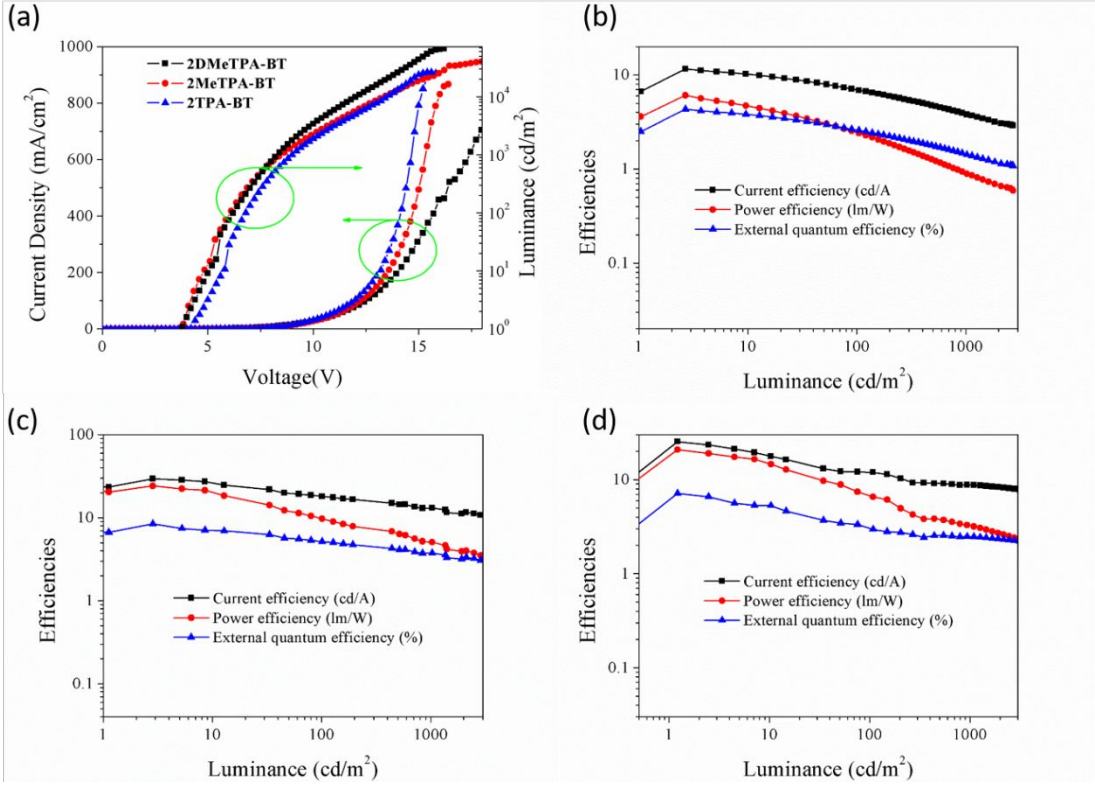

Figure 9. (a) Current density-voltage-luminance curves (*J*-*V*-*L*). Current efficiency-current density (CE-*J*), power efficiency-current density (PE-*J*) and external quantum efficiency-current density (EQE-*J*) curves for (b) **2TPA-BT**, (c) **2MeTPA-BT** and (d) **2DMeTPA-BT**, respectively.

Table 3 Electroluminescence parameters for the three doped devices

Emitters	CE (cd/A) [a]	PE (lm/W) [b]	EQE (%) [c]	L_{max} (cd/m^2) [d]	λ_{EL} (nm) [e]	V_{on} (V) [f]	CIE [g]
2TPA-BT	11.05	6.01	4.43	26767	602	4.2	(0.52, 0.47)
2MeTPA-BT	30.40	23.67	8.47	40151	560	3.8	(0.44, 0.55)
2DMeTPA-BT	25.02	20.37	7.29	64947	544	3.8	(0.38, 0.58)

[a] The maximum current efficiency; [b] The maximum power efficiency; [c] The maximum external quantum efficiency; [d] The maximum luminance; [e] The maximum EL emission peak; [f] Turn-on voltage; [g] Color coordinates

Conclusions

In summary, three D-A-D type small organic emitters of **2TPA-BT**, **2MeTPA-BT** and **2DMeTPA-BT** were rationally designed and synthesized. By introducing steric

hindrance due to methyl groups between the D and A units, different torsional angles between D and A units are observed. These emitters show different emission wavelengths with high Φ_{PL}s in toluene solvent and neat film. The emission of the emitters proved to be governed by an HLCT mechanism. Attributed to the high Φ_{PL}s and HLCT mechanism of the emitters, the related OLEDs gave strong EL with emission peaks at 602, 560 and 544 nm, maximum CEs of 11.05 cd/A, 30.40 cd/A and 25.02 cd/A, maximum PEs of 6.01 lm/W, 23.67 lm/W and 20.37 lm/W, maximum EQEs 4.43%, 8.47% and 7.29% for the **2TPA-BT**, **2MeTPA-BT** and **2DMeTPA-BT** doped OLEDs, respectively. This work clearly illustrates the effect of spatial configuration changes on the luminescence properties of organic emitters.

Experimental Section

Synthesis of N-(4-bromo-3-methylphenyl)-4-*tert*-butyl-N-(4-*tert*-butylphenyl)-benzenamine (MeTPA-Br)

To a mixture of 1-*tert*-butyl-4-iodobenzene (7.56 g, 29.07 mmol), 4-bromo-3-methylbenzenamine (2.46 g, 13.22 mmol) and 1,10-phenanthroline (0.49 g, 2.64 mmol) was added a degassed solvent of toluene (80 mL). After the mixture was heated to 110 ^{o}C under the protection of nitrogen, a mixture of CuI (0.76 g, 4.00 mmol) and KOH (6.00 g, 105 mmol) was added quickly. Then the mixture was further refluxed under 135 ^{o}C for 6 h under the protection of nitrogen. After being cooled to room temperature, the mixture was poured into water (100 mL). It was extracted with dichloromethane (DCM) (3 × 120 mL) and the combined organic layer

was dried over anhydrous magnesium sulfate. The solvent was removed off by rotary evaporation and the residue was passed through a flash silica gel column with petroleum ether (PE)/ (DCM) (*v/v*, 10:1) as the eluent to give a white solid (4.23 g, yield 70.5%). ^{1}H NMR (400 MHz, CD_2Cl_2), δ (ppm): 7.36 (d, J = 8.6 Hz, 1H), 7.30 (d, J = 2.8 Hz, 4H), 7.05–6.98 (m, 4H), 6.97 (d, J = 2.6 Hz, 1H), 6.74 (dd, J = 8.6, 2.7 Hz, 1H), 2.31 (s, 3H), 1.34 (s, 18H). ^{13}C NMR (100 MHz, CD_2Cl_2), δ (ppm):147.57, 146.07, 144.85, 138.37, 132.50, 126.13, 124.92, 123.98, 121.94, 34.18, 30.86, 22.61. ESI-MS (*m/z*) calcd for $C_{27}H_{32}BrN$ $[M]^+$: 450.45. Found: 450.37.

Synthesis of N-(4-bromo-3,5-dimethylphenyl)-4-*tert*-butyl-N-(4-*tert*-butylphenyl) -benzenamine (DMeTPA-Br)

The compound **DMeTPA-Br** was synthesized by the similar synthetic procedure for **MeTPA-Br** with 1-*tert*-butyl-4-iodobenzene (5.23 g, 20.11 mmol) and 4-bromo-3,5-dimethylbenzenamine (1.83 g, 9.14 mmol) as starting materials and obtained as a white solid with a yield of 61% (2.59 g). ^{1}H NMR (400 MHz, $CDCl_3$), δ (ppm): 7.24 (d, J = 8.6 Hz, 4H), 6.97 (d, J = 7.7 Hz, 4H), 6.79 (s, 2H), 2.30 (s, 6H), 1.31 (s, 18H). ^{13}C NMR (100 MHz, $CDCl_3$), δ (ppm): 146.61, 145.53, 144.97, 138.76, 126.04, 123.72, 123.24, 120.02, 34.30, 31.47, 23.92. ESI-MS (*m/z*) calcd for $C_{28}H_{34}BrN$ $[M]^+$: 464.48. Found: 464.60.

Synthesis of 2TPA-BT

To a mixture of **TPA-Br** (1.00 g, 2.29 mmol), **BT-2Bpin** (0.39 g, 1.00 mmol), and tetrakis(triphenylphosphine)palladium ($Pd(PPh_3)_4$, 0.13 g) was added a degassed mixture of toluene (40 mL), anhydrous ethanol (10 mL) and 2 M potassium carbonate

aqueous solution (9 mL). The mixture was refluxed for 23 h under the protection of nitrogen. After being cooled to room temperature, the mixture was poured into water (80 mL). It was extracted with DCM (3 × 80 mL) and the combined organic layer was dried over anhydrous magnesium sulfate. The solvent was removed off by rotary evaporation and the residue was passed through a flash silica gel column with DCM as the eluent to give a red solid (0.49 g, yield 58%). ^{1}H NMR (400 MHz, $CDCl_3$), δ (ppm): 7.88 (d, J = 8.8 Hz, 4H), 7.75 (s, 2H), 7.32 (d, J = 8.4 Hz, 8H), 7.21 (d, J = 7.2 Hz, 4H), 7.14 (d, J = 8.2 Hz, 8H), 1.35 (s, 36H). ^{13}C NMR (101 MHz, $CDCl_3$), δ (ppm) 154.32, 148.31, 146.10, 144.78, 132.15, 130.36, 129.75, 127.28, 126.15, 124.55, 122.16, 34.85, 31.61. MALDI-TOF-MS (*m/z*) calcd for $C_{58}H_{62}N_4S$ $[M]^+$: 846.4695. Found: 846.4709.

Synthesis of 2MeTPA-BT

The compound **2MeTPA-BT** was synthesized by the similar synthetic procedure for **2TPA-BT** with **MeTPA-Br** (1.03 g, 2.29 mmol) and **BT-2Bpin** (0.39 g, 1.00 mmol) as starting materials and obtained as an orange solid with a yield of 50% (0.43 g). ^{1}H NMR (400 MHz, CD_2Cl_2), δ (ppm): 7.59 (s, 2H), 7.37 (d, J = 8.6 Hz, 8H), 7.29 (d, J = 8.4 Hz, 2H), 7.14 (d, J = 8.6 Hz, 8H), 7.08 (d, J = 2.0 Hz, 2H), 6.97 (dd, J = 8.4, 2.2 Hz, 2H), 2.16 (s, 6H), 1.37 (s, 36H). ^{13}C NMR (100 MHz, $CDCl_3$), δ (ppm): 154.43, 148.06, 145.81, 145.00, 137.31, 133.86, 131.09, 130.66, 129.54, 126.16, 124.40, 123.94, 119.86, 34.37, 31.65, 20.80. MALDI-TOF-MS (*m/z*) calcd for $C_{60}H_{66}N_4S$ $[M]^+$: 874.5008. Found: 874.5020.

Synthesis of 2DMeTPA-BT

The compound **2DMeTPA-BT** was synthesized by the similar synthetic procedure for **2TPA-BT** with **DMeTPA-Br** (1.06 g, 2.29 mmol) and **BT-2Bpin** (0.39 g, 1.00 mmol) as starting materials and obtained as a yellow-green solid with a yield of 42% (0.38 g). ^{1}H NMR (400 MHz, $CDCl_3$), δ (ppm): 7.51 (s, 2H), 7.31 (d, J = 8.4 Hz, 8H), 7.15 (d, J = 7.6 Hz, 8H), 6.91 (s, 4H), 1.95 (s, 12H), 1.36 (s, 36H). ^{13}C NMR (101 MHz, $CDCl_3$), δ (ppm):154.58, 147.50, 146.41, 146.25, 145.35, 137.27, 133.25, 130.45, 130.14, 126.00, 124.33, 121.43, 34.07, 31.60, 21.20. MALDI-TOF-MS (*m/z*) calcd for $C_{62}H_{70}N_4S$ $[M]^+$: 902.5321. Found: 902.5298.

X-ray crystallographic analysis

Single crystals of **2TPA-BT**, **2MeTPA-BT** and **2DMeTPA-BT** were obtained by slow diffusion of methanol into their dichloromethane solutions. Suitable crystals were selected and diffraction data were collected on a SuperNova, Dual, Cu at zero, AtlasS2 diffractometer. The crystals were kept at 100.01(10) K during data collection. Complete crystallographic data can be found in CCDC no. 1890911, 1890912 and 1890913 for **2TPA-BT**, **2MeTPA-BT** and **2DMeTPA-BT**, respectively, which can be obtained free from the Cambridge Crystallographic Data Centre (www.ccdc.cam.ac.un/conts/retrieving.html).

Supporting Information

Supporting Information is available from the Wiley Online Library or from the author.

Acknowledgements

This work was financially supported by the National Natural Science Foundation of China (51903157), Hong Kong Research Grants Council (C6009-17G), Hong Kong Polytechnic University (1-ZE1C), the Endowed Professorship in Energy from Ms Clarea Au (847S) and China Postdoctoral Science Foundation Funded Project (2017M622748, 2019T120747).

References

[1] K. Wu, T. Zhang, Z. Wang, L. Wang, L. Zhan, S. Gong, C. Zhong, Z. H. Lu, S. Zhang, C. Yang, *J. Am. Chem. Soc.* 2018, **140**, 8877-8886.

[2] G. Z. Lu, N. Su, H. Q. Yang, Q. Zhu, W. W. Zhang, Y. X. Zheng, L. Zhou, J. L. Zuo, Z. X. Chen, H. J. Zhang, *Chem. Sci.,* 2019, **10**, 3535-3542.

[3] Q.-C. Zhang, H. Xiao, X. Zhang, L.-J. Xu, Z.-N. Chen, *Coord. Chem. Rev.* 2019, **378**, 121-133.

[4] Z. G. Wu, H. B. Han, Z. P. Yan, X. F. Luo, Y. Wang, Y. X. Zheng, J. L. Zuo, Y. Pan, *Adv. Mater.* 2019, **31**, 1900524.

[5] X. Ai, E. W. Evans, S. Dong, A. J. Gillett, H. Guo, Y. Chen, T. J. H. Hele, R. H. Friend, F. Li, *Nature* 2018, **563**, 536-540.

[6] Y. Zhang, Y. Wang, J. Song, J. Qu, B. Li, W. Zhu, W.-Y. Wong, *Adv. Optical Mater.* 2018, **6**, 1800466.

[7] H. Uoyama, K. Goushi, K. Shizu, H. Nomura, C. Adachi, *Nature* 2012, **492**,

234-237.

[8] L. Yao, S. Zhang, R. Wang, W. Li, F. Shen, B. Yang, Y. Ma, *Angew. Chem. Int. Ed.* 2014, **53**, 2119-2123.

[9] N. Su, H.-Q. Yang, C.-Z. Shen, Z.-P. Yan, Z.-X. Chen, Y.-X. Zheng, *J. Mater. Chem. C,* 2019, **7**, 6972-6977.

[10] H. Xiang, J. Cheng, X. Ma, X. Zhou, J. J. Chruma, *Chem. Soc. Rev.,* 2013, **42**, 6128-6185.

[11] K. Tuong Ly, R.-W. Chen-Cheng, H.-W. Lin, Y.-J. Shiau, S.-H. Liu, P.-T. Chou, C.-S. Tsao, Y.-C. Huang, Y. Chi, *Nat. Photonics* 2016, **11**, 63-68.

[12] Z. Yang, Z. Mao, Z. Xie, Y. Zhang, S. Liu, J. Zhao, J. Xu, Z. Chi, M. P. Aldred, *Chem. Soc. Rev.,* 2017, **46**, 915-1016.

[13] J. Guo, X.-L. Li, H. Nie, W. Luo, S. Gan, S. Hu, R. Hu, A. Qin, Z. Zhao, S.-J. Su, B. Z. Tang, *Adv. Funct. Mater.* 2017, **27**, 1606458.

[14] M. Y. Wong, E. Zysman-Colman, *Adv. Mater.* 2017, **29**, 1605444.

[15] B. Liu, Z.-W. Yu, D. He, Z.-L. Zhu, J. Zheng, Y.-D. Yu, W.-F. Xie, Q.-X. Tong, C.-S. Lee, *J. Mater. Chem. C,* 2017, **5**, 5402-5410.

[16] W. C. Chen, Y. Yuan, S. F. Ni, Q. X. Tong, F. L. Wong, C. S. Lee, *Chem. Sci.,* 2017, **8**, 3599-3608.

[17] J. Xue, Q. Liang, Y. Zhang, R. Zhang, L. Duan, J. Qiao, *Adv. Funct. Mater.* 2017, **27**, 1703283.

[18] X. Ai, Y. Chen, Y. Feng, F. Li, *Angew. Chem. Int. Ed.* 2018, **57**, 2869-2873.

[19] S. Wang, X. Yan, Z. Cheng, H. Zhang, Y. Liu, Y. Wang, *Angew. Chem. Int. Ed.*

2015, **54**, 13068-13072.

[20] C. Li, R. Duan, B. Liang, G. Han, S. Wang, K. Ye, Y. Liu, Y. Yi, Y. Wang, *Angew. Chem. Int. Ed.* 2017, **56**, 11525-11529.

[21] P. Data, P. Pander, M. Okazaki, Y. Takeda, S. Minakata, A. P. Monkman, *Angew. Chem. Int. Ed*. 2016, **55**, 5739-5744.

[22] A. Klimash, P. Pander, W. T. Klooster, S. J. Coles, P.Data, F. B. Dias, P. J. Skabara, *J. Mater. Chem. C*, 2018, **6**, 10557-10568.

[23] P. K. Samanta, D. Kim, V. Coropceanu, J. L. Bredas, *J. Am. Chem. Soc.* 2017, **139**, 4042-4051.

[24] L. S. Cui, H. Nomura, Y. Geng, J. U. Kim, H. Nakanotani, C. Adachi, *Angew. Chem. Int. Ed.* 2017, **56**, 1571-1575.

[25] M. Okazaki, Y. Takeda, P. Data, P. Pander, H. Higginbotham, A. P. Monkman, S. Minakata, *Chem. Sci.,* 2017, **8**, 2677-2686.

[26] W. Zeng, H. Y. Lai, W. K. Lee, M. Jiao, Y. J. Shiu, C. Zhong, S. Gong, T. Zhou, G. Xie, M. Sarma, K. T. Wong, C. C. Wu, C. Yang, *Adv. Mater.* 2018, **30**, 1704961.

[27] T. Liu, L. Zhu, C. Zhong, G. Xie, S. Gong, J. Fang, D. Ma, C. Yang, *Adv. Funct. Mater.* 2017, **27**, 1606384.

[28] B. Li, L. Zhou, H. Cheng, Q. Huang, J. Lan, L. Zhou, J. You, *Chem. Sci.,* 2018, **9**, 1213-1220.

[29] C. Wang, X.-L. Li, Y. Gao, L. Wang, S. Zhang, L. Zhao, P. Lu, B. Yang, S.-J. Su, Y. Ma, *Adv. Optical Mater.* 2017, **5**, 1700441.

[30] J. Yang, Q. Guo, J. Wang, Z. Ren, J. Chen, Q. Peng, D. Ma, Z. Li, *Adv. Optical Mater.* 2018, **6**, 1800342.

[31] M. A. Topchiy, A. F. Asachenko, M. S. Nechaev, *Eur. J. Org. Chem.* 2014, 3319-3322.

[32] Y. Zhang, X. Bao, M. Xiao, H. Tan, Q. Tao, Y. Wang, Y. Liu, R. Yang, W. Zhu, *J. Mater. Chem. A,* 2015, **3**, 886-893.

[33] C. M. Cardona, W. Li, A. E. Kaifer, D. Stockdale, G. C. Bazan, *Adv. Mater.* 2011, **23**, 2367-2371.

[34] C. J. Yao, J. Yao, Y. W. Zhong, *Inorg. Chem.* 2011, **50**, 6847-6849.

[35] Y. Zhang, Z. Chen, J. Song, J. He, X. Wang, J. Wu, S. Chen, J. Qu, W.-Y. Wong, *J. Mater. Chem. C*, 2019, **7**, 1880-1887.

[36] Y. Zhang, J. Wu, J. Song, Z. Chen, J. He, X. Wang, H. Liu, S. Chen, J. Qu, W.-Y. Wong, *Adv. Electron. Mater.* 2019, **5**, 1800677.

[37] V. E. Z. Lippert, *Electrochemistry* 1957, **61**, 962-975.

[38] N. Mataga, Y. Kaifu, M. Koizumi, *Bull. Chem. Soc. Jpn*. 1956, **29**, 465-470.

[39] E. Bozkurt, H. I. Gul, E. Mete, *J. Photochem. Photobiol A: Chem.* 2018, **352**, 35-42.

[40] S. Kothavale, N. Sekar, *Dyes Pigm.* 2017, **136**, 31-45.

[41] Gaussian 09, Revision D.01, M. J. Frisch, G. W. Trucks, H. B. Schlegel, G. E. Scuseria, M. A. Robb, J. R. Cheeseman, G. Scalmani, V. Barone, B. Mennucci, G. A. Petersson, H. Nakatsuji, M. Caricato, X. Li, H. P. Hratchian, A. F. Izmaylov, J. Bloino, G. Zheng, J. L. Sonnenberg, M. Hada, M. Ehara, K. Toyota,

R. Fukuda, J. Hasegawa, M. Ishida, T. Nakajima, Y. Honda, O. Kitao, H. Nakai, T. Vreven, J. A. Montgomery, J. E. Peralta, F. Ogliaro, M. Bearpark, J. J. Heyd, E. Brothers, K. N. Kudin, V. N. Staroverov, T. Keith, R. Kobayashi, J. Normand, K. Raghavachari, A. Rendell, J. C. Burant, S. S. Iyengar, J. Tomasi, M. Cossi, N. Rega, J. M. Millam, M. Klene, J. E. Knox, J. B. Cross, V. Bakken, C. Adamo, J. Jaramillo, R. Gomperts, R. E. Stratmann, O. Yazyev, A. J. Austin, R. Cammi, C. Pomelli, J. W. Ochterski, R. L. Martin, K. Morokuma, V. G. Zakrzewski, G. A. Voth, P. Salvador, J. J. Dannenberg, S. Dapprich, A. D. Daniels, O. Farkas, J. B. Foresman, J. V. Ortiz, J. Cioslowski and D. J. Fox, Gaussian, Inc., Wallingford CT, 2013.